

LEARNING MIXTURES OF LINEAR DYNAMICAL SYSTEMS (MoLDS) VIA HYBRID TENSOR–EM METHOD

Lulu Gong, Shreya Saxena

Department of Biomedical Engineering

Wu Tsai Institute Center for Neurocomputation and Machine Learning

Yale University, New Haven, CT, 06510, USA

{lulu.gong@yale.edu}

ABSTRACT

Linear dynamical systems (LDSs) have been powerful tools for modeling high-dimensional time-series data across many domains, including neuroscience. However, a single LDS often struggles to capture the heterogeneity of neural data, where trajectories recorded under different conditions can have variations in their dynamics. Mixtures of linear dynamical systems (MoLDS) provide a path to model these variations in temporal dynamics for different observed trajectories. However, MoLDS remains difficult to apply in complex and noisy settings, limiting its practical use in neural data analysis. Tensor-based moment methods can provide global identifiability guarantees for MoLDS, but their performance degrades under realistic noise and complexity. Commonly used expectation–maximization (EM) methods offer flexibility in fitting latent models but are highly sensitive to initialization and prone to poor local minima. Here, we propose a tensor-based moment method that provides identifiability guarantees for learning MoLDS, which can be followed by EM updates to combine the strengths of both approaches. The novelty in our approach lies in the construction of moment tensors using the input–output data, on which we then apply Simultaneous Matrix Diagonalization (SMD) to recover globally consistent estimates of mixture weights and system parameters. These estimates can then be refined through a full Kalman Filter-Smoother EM algorithm, with closed-form updates for all LDS parameters. We validate our framework on synthetic benchmarks and real-world datasets. On synthetic data, the proposed Tensor-EM method achieves more reliable recovery and improved robustness compared to either pure tensor or randomly initialized EM methods. We then analyze neural recordings from the primate somatosensory cortex while a non-human primate performs reaches in different directions. In this setting, our method successfully models and clusters different conditions as separate subsystems, which is consistent with supervised single-LDS fits for each condition. Finally, we apply this approach to another neural dataset where monkeys perform a sequential reaching task. These results demonstrate that MoLDS provides an effective framework for modeling complex neural data in different brain regions, and that Tensor-EM is a principled and reliable approach to MoLDS learning for these applications.

1 INTRODUCTION

Neuroscience experiments now produce large volumes of high-dimensional time-series datasets, calling for new computational tools to uncover the dynamical principles underlying brain function Paninski & Cunningham (2018); Stringer & Pachitariu (2024); Urai et al. (2022). These recorded data often originate from multiple, distinct underlying dynamical processes, yet the identity of the generating system at any given time is unknown. Estimating and recovering the parameters and dynamics of such latent systems from these mixed neural trajectories is a central challenge in system identification and machine learning Ljung (1998); Durbin & Koopman (2012); Bishop (2006).

Classical mixture models, such as mixtures of Gaussians (MoG) Dempster et al. (1977) and mixtures of linear regressions (MLR) De Veaux (1989), provide valuable tools for modeling these heteroge-

neous data. However, they are primarily designed for static settings and do not explicitly capture temporal dependencies, limiting their applicability to sequential data where temporal dynamics are central. In contrast, dynamical models such as linear dynamical systems (LDS) and their extensions-(recurrent) switching LDS (SLDS) Ghahramani & Hinton (2000); Fox (2009); Linderman et al. (2017)-are suitable for time-series data modeling with latent states and regime switches. Switching models typically target a single long trajectory and are prone to solutions that contain frequent switching; they often underperform when the goal is to learn parameters of multiple distinct LDSs from independent trials, which is precisely the structure common in neural experiments.

Mixtures of linear dynamical systems (MoLDS)Chen & Poor (2022); Bakshi et al. (2023) effectively address this setting by treating each trajectory as originating from a single latent LDS. Inference of MoLDS aims to uncover the number of subsystems, their parameters, and the mixture weights from collections of input–output trajectories. This formulation enables direct parameter recovery and interpretability, making it appealing for applications such as neural data analysis, where multiple distinct but repeated dynamical motifs are observed across trials.

For inference of MoLDS, tensor-based moment methods are commonly employed, where high-order statistical moments of the input–output data are reorganized into structured tensors, and their decomposition provides estimates of mixture weights and LDS parameters. The appeal of these algebraic approaches lies in their global identifiability: unlike iterative optimization methods that navigate non-convex landscapes, tensor decomposition exploits the algebraic structure of moments to directly recover parameters through polynomial equation systems that admit unique solutions under ideal conditions Anandkumar et al. (2014). However, their practical performance is often limited because moment estimates become imperfect in realistic, noisy datasets, leading to degraded parameter recovery. In parallel, likelihood-based approaches such as expectation–maximization (EM) have long been widely used for fitting classical mixture models and SLDS. EM provides a flexible iterative procedure for jointly estimating latent states, mixture weights, and system parameters through local likelihood optimization. While powerful and widely adopted, EM suffers from well-known sensitivity to initialization and susceptibility to poor local minima-limitations that become particularly problematic in the MoLDS setting, where the parameter space is high-dimensional and the likelihood surface is highly multimodal.

Here, we propose a hybrid Tensor-EM framework that strategically combines global initialization with local refinement for MoLDS. We first apply tensor decomposition based on *Simultaneous Matrix Diagonalization* (SMD) to obtain stable and accurate initial estimates. We then use these estimates to initialize a full *Kalman Filter–Smooother EM* procedure, which refines all parameters through closed-form updates. This hybrid approach harnesses the global identifiability of tensor methods for robust initialization, while leveraging EM’s superior local optimization, to achieve both reliability and accuracy.

We validate this framework on both synthetic and real-world datasets. On synthetic benchmarks, the proposed Tensor-EM method achieves more reliable recovery and improved robustness compared to pure tensor methods and EM with random initialization. Next, we analyze neural recordings from two different experiments. (1) Recordings from monkey somatosensory cortex during center-out reaches in different directions, where Tensor-EM identifies distinct dynamical clusters corresponding to the reaching directions, matching supervised LDS fits per direction but achieved in a fully unsupervised manner. (2) Recordings from the dorsal premotor cortex while a monkey performs reaches in continuously distributed directions, where Tensor-EM succeeds in parsing the different trials into direction-specific dynamical models. These results establish MoLDS as an effective framework for modeling heterogeneous neural systems, and demonstrate that Tensor-EM provides a principled and reliable solution for learning MoLDS in both synthetic and challenging real-world settings.

2 RELATED WORK

Mixtures models. Mixture models (e.g., MoG and MLR) capture heterogeneity but not explicit temporal structure Dempster et al. (1977); De Veaux (1989); Li & Liang (2018). MoLDS offers fundamental advantages over classical mixture models for modeling complex temporal phenomena. Importantly, MoLDS is related to MLR through lagged-input representations: by augmenting inputs with their past values, an MLR model can approximate certain temporal dependencies. Through this connection, MoLDS inherits useful algorithmic tools, including spectral tensor methods and

optimization approaches Anandkumar et al. (2014); Yi et al. (2016); Pal et al. (2022); Li & Liang (2018), while maintaining its superior modeling capacity for dynamical systems.

Tensor methods and EM. Tensor decomposition methods offer a principled algebraic approach to parameter estimation in latent variable models, with polynomial-time algorithms and theoretical identifiability guarantees Anandkumar et al. (2014). Recent work in tensor-based MoLDS learning has explored different moment construction strategies and decomposition algorithms. Early approaches applied Jennrich’s algorithm directly to input-output moments Bakshi et al. (2023), while more recent work incorporates temporal lag structure using the MLR reformulation and the robust tensor power method Rui & Dahleh (2025). Our approach adopts Simultaneous Matrix Diagonalization (SMD) Kuleshov et al. (2015) for tensor decomposition, which operates on whitened tensor slices and offers improved numerical stability and robustness to noise-critical advantages in the challenging MoLDS setting.

The combination of tensor initialization followed by EM-style refinement has proven effective in mixture model settings. In the MLR literature, tensor methods provide globally consistent initial estimates that lie within the basin of attraction of the maximum likelihood estimator, which are then refined using alternating minimization Yi et al. (2016); Zhong et al. (2016); Chen et al. (2021). However, alternating minimization represents a simplified version of EM that uses hard assignments rather than the probabilistic responsibilities essential for handling uncertainty in noisy settings. Our work extends this paradigm to the more complex MoLDS setting by combining tensor initialization with full Kalman filter-smoother EM, including proper handling of latent state inference and closed-form parameter updates.

Contributions. Our work makes both methodological and empirical contributions to MoLDS learning and shows its practical utility in neuroscience settings. Methodologically, relative to existing MoLDS tensor methods, our approach makes several key advances: (i) we employ SMD for more stable decomposition of whitened moment tensors, (ii) we provide a principled initialization strategy for noise parameters (Q, R) based on residual covariances, which was missing from prior tensor-based approaches, and (iii) we integrate a complete EM procedure with responsibility-weighted sufficient statistics for all LDS parameter updates. Compared to existing tensor-alternating minimization pipelines for MLR, our method leverages the full complexity of Kalman filtering and smoothing, which is essential for addressing the temporal dependencies and uncertainty quantification required in MoLDS applications. Empirically, we demonstrate the successful applications of tensor-based MoLDS methods to complex and real-world data analysis. While prior MoLDS tensor work has been limited to synthetic evaluations, we show that our Tensor-EM framework can effectively analyze neural recordings from primate somatosensory cortex during reaching tasks, successfully identifying distinct dynamical regimes corresponding to different movement directions in a fully unsupervised manner. This represents an important step toward making MoLDS a practical tool for important applications such as neuroscience, where capturing heterogeneous dynamics across experimental conditions is a central challenge. Together, these methodological and empirical advances demonstrate that our Tensor-EM MoLDS framework provides improved robustness and accuracy in both controlled and challenging real-world settings.

3 MOLDS: MODEL AND TENSOR-EM METHOD

3.1 MIXTURE OF LINEAR DYNAMICAL SYSTEMS (MoLDS)

In the MoLDS setting, we observe N input–output trajectories $\{(u_{i,0:T_i-1}, y_{i,0:T_i-1})\}_{i=1}^N$, each generated by one of K latent LDS components. Let $z_i \in [K]$ denote the (unknown) component for trajectory i , drawn i.i.d. as $z_i \sim \text{Multinomial}(p_{1:K})$, where $p_k \in (0, 1)$ are the mixture weights with $\sum_{k=1}^K p_k = 1$, indicating the probability of a trajectory being generated by component k . Conditional on $z_i = k$, the data is generated from the following LDS:

$$x_{t+1} = A_k x_t + B_k u_t + w_t, \quad w_t \sim \mathcal{N}(0, Q_k), \quad (1)$$

$$y_{t+1} = C_k x_t + D_k u_t + v_t, \quad v_t \sim \mathcal{N}(0, R_k), \quad (2)$$

with $A_k \in \mathbb{R}^{n \times n}$, $B_k \in \mathbb{R}^{n \times m}$, $C_k \in \mathbb{R}^{p \times n}$, $D_k \in \mathbb{R}^{p \times m}$, and $Q_k \succeq 0$, $R_k \succeq 0$. The goal of MoLDS learning is to recover the mixture weights and LDS parameters $\{p_k, (A_k, B_k, C_k, D_k, Q_k, R_k)\}_{k=1}^K$. These parameters are identifiable only up to two natural ambiguities: the ordering of the compo-

nents (permutation) and similarity transformations of the latent state realization (which leave the input–output behavior unchanged).¹

To make this recovery possible, we adopt several standard conditions: (i) inputs are persistently exciting, (ii) each LDS component is controllable and observable, and (iii) the components are sufficiently separated to ensure identifiability Bakshi et al. (2023); Rui & Dahleh (2025).

3.2 TENSOR-EM APPROACH OVERVIEW

Our approach (Algorithm 1) consists of two stages: a tensor initialization stage (see Algorithm 3 in the Appendix), which provides globally consistent estimates of the mixture weights and system parameters, and an EM refinement stage (see Algorithm 4), which further improves these estimates to achieve statistical efficiency. Between these two stages, a key step is the initialization of the noise parameters (Q_k, R_k) , since these are not identifiable from the tensor-based estimates. We address this gap by estimating them from the residual covariances computed using the tensor-based parameter estimates (detailed in Appendix C).

This Tensor-EM approach combines the global identifiability guarantees of algebraic methods with the statistical optimality of likelihood-based inference. This hybrid approach is particularly effective in challenging settings with limited data, high noise, or poor component separation—scenarios where neither pure tensor methods nor randomly initialized EM perform reliably.

Algorithm 1 Tensor-EM Pipeline for MoLDS

Require: Trajectories $\{(u_{i,0:T_i-1}, y_{i,0:T_i-1})\}_{i=1}^N$, truncation L , LDS order n , #components K
Ensure: Mixture weights $\{\hat{p}_k\}_{k=1}^K$ and LDS parameters $\{(\hat{A}_k, \hat{B}_k, \hat{C}_k, \hat{D}_k, \hat{Q}_k, \hat{R}_k)\}_{k=1}^K$ (Appendix Alg. 3)
Stage 1: Tensor Initialization (Appendix Alg. 3)
1: Transform MoLDS to MLR via lagged inputs; construct moment tensors M_2, M_3
2: Apply whitening and SMD to recover mixture weights $\{\hat{p}_k\}$ and Markov parameters
3: Realize LDS matrices $\{(\hat{A}_k, \hat{B}_k, \hat{C}_k, \hat{D}_k)\}$ via Ho-Kalman algorithm
4: Initialize noise parameters $\{(\hat{Q}_k^{(0)}, \hat{R}_k^{(0)})\}$ from residual covariances (Appendix C)
Stage 2: EM Refinement (Appendix Alg. 4)
5: **repeat**
6: **E-step:** Compute trajectory responsibilities $\gamma_{i,k}$ via Kalman filter likelihoods
7: Run Kalman smoother to obtain responsibility-weighted sufficient statistics
8: **M-step:** Update mixture weights and all LDS parameters via closed-form MLE
9: **until** convergence in log-likelihood
10: **return** Refined parameters $\{\hat{p}_k, (\hat{A}_k, \hat{B}_k, \hat{C}_k, \hat{D}_k, \hat{Q}_k, \hat{R}_k)\}_{k=1}^K$

3.3 TENSOR INITIALIZATION FOR MoLDS

The tensor initialization leverages the key insight that MoLDS can be reformulated as MLR through lagged input representations. This transformation exposes the mixture structure in high-order moments, enabling algebraic recovery of component parameters via tensor decomposition (see Appendix A for details). The method works by exploiting the impulse-response (Markov parameter) representation of LDSs. We construct second- and third-order cross moments of the lagged input–output data, denoted M_2 and M_3 (see Appendix A.2). Then we apply whitening transformations and decompose the resulting tensor into weights and Markov parameter estimates. At last, we recover LDS state-space parameters through the Ho-Kalman realization Oymak & Ozay (2019). The core mathematical insight is that if M_2 and M_3 are appropriately constructed from sub-sampled lagged covariates, the whitened tensor

$$\widehat{T} = M_3(W, W, W) = \sum_{k=1}^K p_k \alpha_k^{\otimes 3} \quad (3)$$

¹Formally, any invertible matrix M induces an equivalent realization via $A_k \mapsto M^{-1} A_k M$, $B_k \mapsto M^{-1} B_k$, $C_k \mapsto C_k M$, and D_k unchanged, yielding the same input–output mapping.

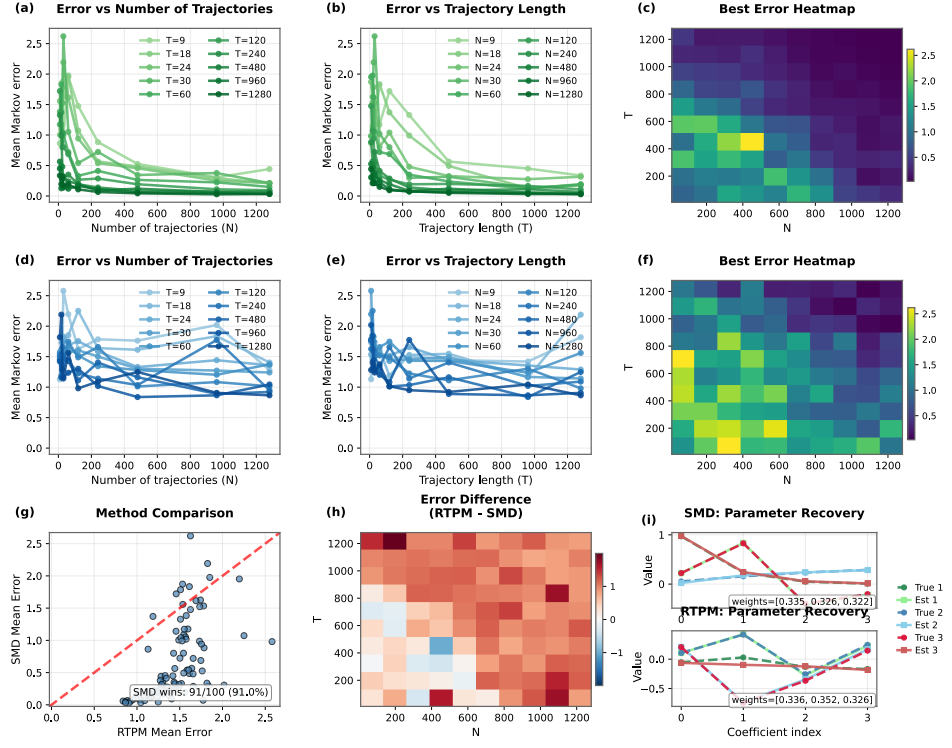


Figure 1: **Comparison of SMD-Tensor and RTPM-Tensor methods for MoLDS.** (a,b) Mean Markov parameter estimation errors for the SMD method decrease as the number of trajectories as N and/or T increase; (c) Heatmap of the best trial result across all (N, T) configurations. (d–f) Corresponding results for the RTPM method. (g) Difference in mean Markov errors between RTPM and SMD (positive values indicate SMD performs better). (h) Scatter plot comparing mean Markov errors of RTPM vs. SMD across configurations, with SMD outperforming in 91% of cases. (i) Example recovery for $N = T = 1280$, where SMD recovers both mixture weights and Markov parameters more accurately.

is symmetric and orthogonally decomposable, where $\alpha_k \in \mathbb{R}^K$ are the whitened representations of the regression vectors (scaled Markov parameters) for each LDS component, and p_k are the corresponding mixture weights. This decomposition is unique and recovers the mixture components $\{\alpha_k, p_k\}$ up to permutation and sign. Importantly, we employ SMD for this decomposition, which is empirically shown to be more stable in Section 4.1. We then apply the Ho-Kalman realization Oymak & Ozay (2019) to recover the state-space parameters for each component, which are then used as principled initializations for the subsequent refinement stage. The complete procedure is provided in Algorithm 3 in Appendix A.4, together with the MoLDS-to-MLR reformulation and tensor construction details in Appendix A.

3.4 EM REFINEMENT FOR MOLDS

The tensor initialization provides globally consistent estimates of mixture weights and system matrices, but does not recover the noise parameters (Q_k, R_k) nor achieve optimal statistical accuracy. We therefore need to refine these estimates using a full Kalman EM algorithm that maximizes the observed-data likelihood.

Our EM formulation extends classical EM to the MoLDS setting by computing trajectory-wise responsibilities via Kalman filter likelihoods, then updating parameters from responsibility-weighted sufficient statistics (see Appendix B and Algorithm 4 for details). In brief, at iteration t , given current

parameters $\hat{\theta}^{(t)} = \{(\hat{p}_k, \hat{A}_k, \hat{B}_k, \hat{C}_k, \hat{D}_k, \hat{Q}_k, \hat{R}_k)\}_{k=1}^K$, the E-step computes responsibilities

$$\gamma_{i,k}^{(t)} = \frac{\exp(\log \hat{p}_k^{(t)} + \log p(y_{i,0:T_i-1} | u_{i,0:T_i-1}, \hat{\theta}_k^{(t)}))}{\sum_{r=1}^K \exp(\log \hat{p}_r^{(t)} + \log p(y_{i,0:T_i-1} | u_{i,0:T_i-1}, \hat{\theta}_r^{(t)}))}. \quad (4)$$

Next, we use a Kalman smoother to compute responsibility-weighted sufficient statistics $S_k^{(t)}$ for each component. The M-step then updates all parameters via closed-form maximum likelihood estimates

$$(\hat{A}_k^{(t+1)}, \hat{B}_k^{(t+1)}, \hat{C}_k^{(t+1)}, \hat{D}_k^{(t+1)}, \hat{Q}_k^{(t+1)}, \hat{R}_k^{(t+1)}) = \text{MLE-LDS}(S_k^{(t)}), \quad (5)$$

$$\hat{p}_k^{(t+1)} = \frac{1}{N} \sum_i \gamma_{i,k}^{(t)}, \quad \forall k \in [K]. \quad (6)$$

4 TENSOR-EM PERFORMANCE ON SYNTHETIC DATA

4.1 SMD-TENSOR METHOD PROVIDES MORE RELIABLE RECOVERY ON SIMULATED MoLDS

We demonstrate that the employed SMD–Tensor method reliably recovers parameters in synthetic MoLDS with a small number of components, low latent dimensionality, and well-separated dynamics. We empirically compare SMD–Tensor against the RTPM–Tensor baseline across a wide range of such settings. Our results show that SMD–Tensor consistently outperforms RTPM–Tensor on multiple metrics. In particular, when the number of mixture components is small and sufficient data are available, SMD achieves near-optimal recovery of both the mixture weights and the Markov parameters.

The first row of Figure 1 reports results of the SMD–Tensor method for a $K = 3$ mixture model with LDS dimensions $n = 2, m = p = 1$. The LDS parameters are randomly generated, with eigenvalues of A constrained to lie inside the unit circle. We vary the trajectory length T and the number of trajectories N , and for each (N, T) configuration. We run multiple independent trials, calculating the discrepancy between estimated and true Markov parameters. The second row of Figure 1 shows the result for RTPM–Tensor. It is noticed that the mean Markov parameter errors decrease with increasing trajectory length and number of trajectories for both methods, but the trend is more pronounced and stable for SMD, as reflected in the heat maps (Figure 1(c,f)). Across nearly all (N, T) cases, SMD yields consistently lower errors (Figures 1(g,h)). In cases with larger T and N , SMD achieves highly accurate recovery of both mixture weights and Markov parameters (Figure 1(c1)), underscoring its robustness and reliability for more complex conditions.

4.2 TENSOR-EM IMPROVES ROBUSTNESS AND ACCURACY FOR COMPLEX SYNTHETIC MoLDS

In complex MoLDS settings with many components, purely tensor-based methods and randomly initialized EM often fail to achieve accurate recovery, either due to noisy parameter estimates or convergence to poor local optima. Our proposed Tensor–EM approach overcomes these limitations by combining globally consistent tensor initialization with EM-based refinement, resulting in more robust and accurate learning. We demonstrate these advantages in this section.

Figure 2 presents results on a simulated $K = 6$ MoLDS ($n = 3, m = p = 2$) with zero direct feedthrough ($D = 0$). Across metrics including Markov parameter errors, mixture weight errors, aggregate LDS parameter errors, and iteration counts, Tensor-EM consistently outperforms all baselines. It achieves substantially lower Markov and weight errors (panels b and c), while maintaining an aggregate parameter error comparable to the pure tensor solution (panel d).² At the same time, Tensor-EM converges in much fewer iterations than random EM (e), leading to a better error-efficiency tradeoff (f). The radar plot (a) summarizes these improvements, showing that Tensor-EM achieves the most balanced performance across all evaluation metrics. These results highlight that Tensor-EM effectively combines the strengths of tensor methods and EM and enable more reliable parameter recovery in synthetic MoLDS settings where standalone tensor or randomly initialized EM approaches often underperform.

²The aggregate parameter error, i.e., the geometric mean of A, B, C errors, is a coarse summary: unlike Markov parameter errors, it may be less precise since A, B, C can differ by similarity transformations without altering the underlying dynamics.

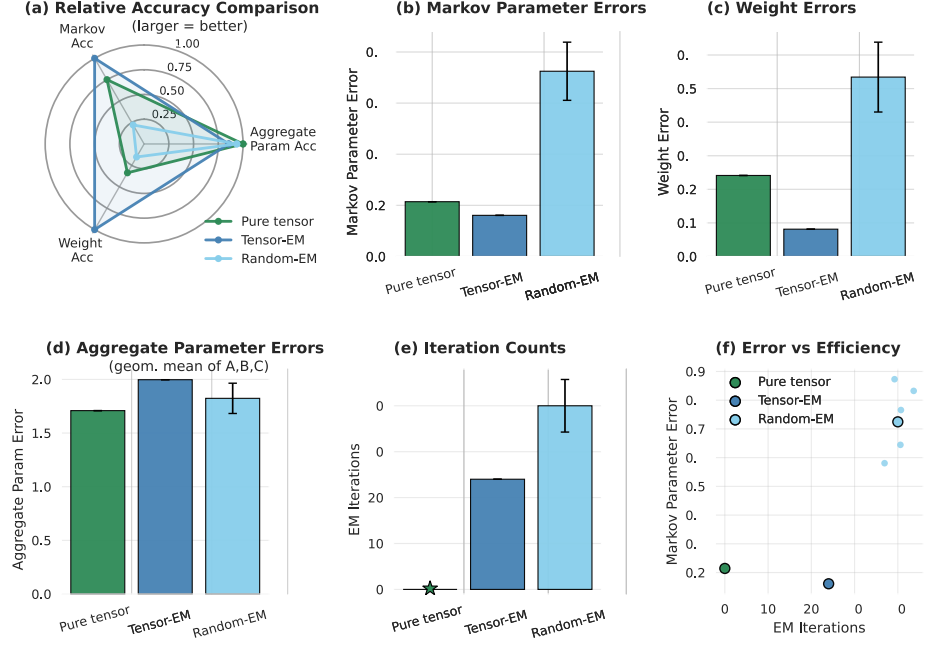


Figure 2: Performance comparison of pure tensor, Tensor-EM, and random-initialized EM on a simulated MoLDS. (a) Relative accuracy radar plot across metrics of Markov parameter accuracy, weight accuracy, and aggregate parameter accuracy. (b-c) Tensor-EM achieves the lowest Markov parameter and weight errors, while random EM performs the worst and shows high variability. (d) reports aggregate parameter errors (geometric mean of A, B, C errors). (e) Tensor-EM converges in far fewer iterations than random EM, highlighting efficiency. (f) Error-efficiency plot shows that Tensor-EM combines low error with moderate iteration cost, yielding robust and accurate recovery.

5 TENSOR-EM MoLDS PROVIDES RELIABLE AND INTERPRETABLE RECOVERY ON REAL-WORLD APPLICATIONS

We next apply the proposed MoLDS method to two real-world neural datasets. Figure 3 gives an overview of the approach and examples from these two datasets.

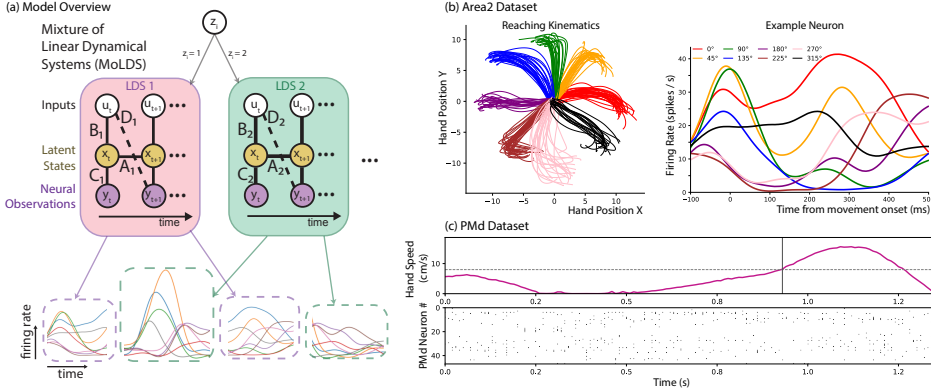


Figure 3: Overview of MoLDS and its applications: (a) Schematic of the MoLDS model structure; MoLDS models observed trajectories as emanating from a set of LDS's. (b) The Area2 Dataset contains neural trajectories from monkey primary somatosensory cortex; reach trajectories and firing rate from an example neuron. (c) The PMd Dataset contains recordings from monkey dorsal premotor cortex; hand speed and neurons' rasters.

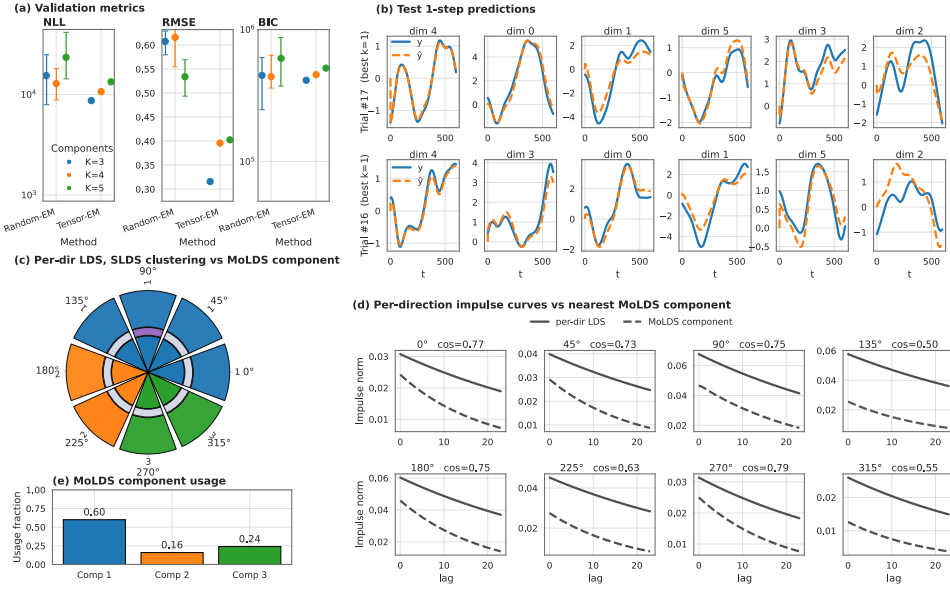


Figure 4: MoLDS application on Area2 Dataset: (a) Validation metrics for different K . (b) One-step predictions for two example trials using corresponding LDS components of the MoLDS selected by the lowest validation metrics. (c) Agreement between MoLDS trial assignments (outer ring) and per-direction single-LDS clusters (inner ring); the SLDS-based method (middle ring) cannot provide correct cross-trial clusters. (d) Per-direction impulse response (Markov parameter) curves for assigned MoLDS component vs. the corresponding single-LDS (titles report cosine similarity). (e) MoLDS component usage fractions on held-out test trials.

5.1 AREA2 DATASET

We first employ a neural dataset from a single recording session of a macaque performing center-out reaches, with neural activity recorded from the somatosensory cortex. During the experiment, the monkey used a manipulandum to direct a cursor from the center of a display to one of eight targets, and neural activity was recorded from Brodmann’s area2 of the somatosensory cortex (see Chowdhury et al. (2020) for experimental details, and Miller (2022) for dataset location). The neural recordings consist of 65 single-unit spike times, which are converted to spike rates. In addition to neural data, the position of the monkey’s hand, cursor position, force applied to the manipulandum, and hand velocity were recorded during the experiment. For our MoLDS setting, we take the hand velocity variables as inputs, and the 65-dim observations are reduced to 6-dim and are regarded as outputs for simplicity by using the standard PCA. There are 8 directions in the task (as shown in Figure 3 (b)), and each direction has multiple trials of input-output trajectories.

We evaluate the MoLDS with Tensor-EM and Random-EM methods using a standard train/validation/test split of the dataset (see full pipeline in App. D). For each hyperparameter setting (including K), models are trained on the training set and scored on the validation set using negative log-likelihood (NLL), one-step-ahead RMSE, and BIC. The model used for test-time analysis is the one minimizing validation BIC (we also report NLL/RMSE). For trial i and component k , we compute a responsibility $r_{ik} \propto \exp(\ell_k^{(i)})$, where $\ell_k^{(i)}$ is the one-step Kalman log-likelihood under component k . For each movement direction, the dominant component is the $\arg \max_k$ of the mean responsibility across its trials.

Figure 4 summarizes results. As shown in Fig. 4(a), validation criteria consistently favor a 3-component MoLDS trained with Tensor-EM. (b) Test one-step predictions \hat{y}_t closely track observations y . (c) Dominant-component maps reveal three cross-trial clusters aligned with direction; (e) usage fractions quantify prevalence on the test set.

In this setup, we also compare Tensor-EM method with the supervised learning results of LDS, where we train one LDS on all trials under each direction. The per-direction LDS baseline closely matches

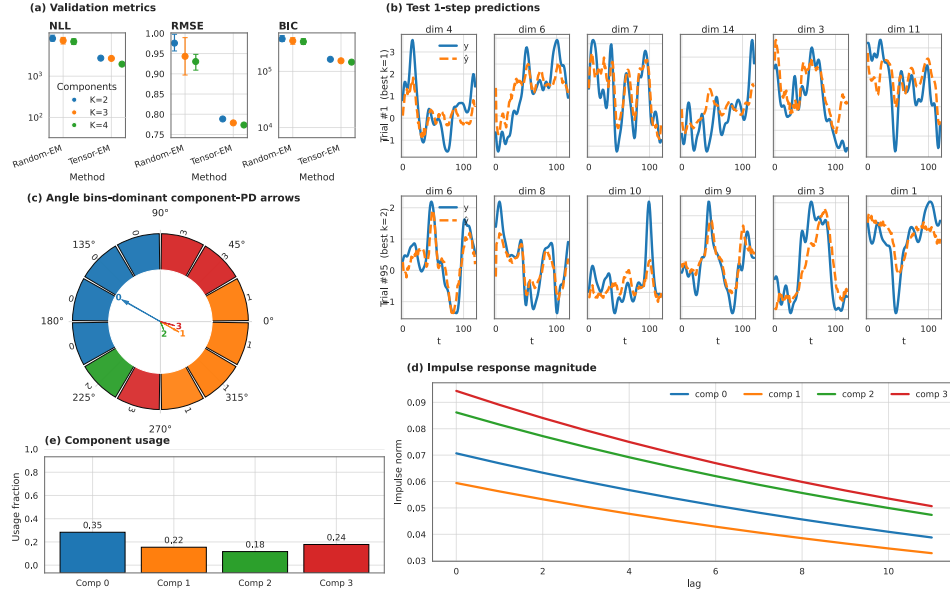


Figure 5: MoLDS application on PMd Dataset: (a) Validation metrics for different K (NLL, RMSE, BIC). (b) Test one-step predictions from the validation-chosen MoLDS. (c) Angle bins: dominant component; PD arrows (responsibility-weighted). (d) Impulse response magnitude of MoLDS components. (e) MoLDS component usage fractions on held-out test trials.

MoLDS-both in impulse responses (high cosine similarity) and in trial groupings (Fig. 4c-d). We also train an SLDS in a similar unsupervised way of MoLDS (no direction labels) and find that it does not yield meaningful cross-trial clusters here, while it is effective for within-trial regime switches (see Figure 6 in Appendix). These highlight MoLDS’s strength in capturing between-trial heterogeneity. Importantly, when compared with the Random-EM method, Tensor-EM offers a key advantage: the tensor initialization step yields a stable starting point that reduces variability across runs, leading to more consistent parameter recovery and model structure as seen in Figure 4(a).

5.2 PMD DATASET

We next evaluate our method on recordings from monkey dorsal premotor cortex (PMd) during more complex reaches, in which trial-wise movement directions are *continuously distributed* over the circle. Full experimental details are in Lawlor et al. (2018b) and the dataset is provided in Perich et al. (2018). The trials’ reach direction spans the full polar range rather than discrete directions as in the Area2 dataset. We analyze PMd activity with the 5-dimensional kinematic as inputs, i.e., (x-velocity, y-velocity, x-acceleration, y-acceleration, speed).

Following the Area2 protocol, we train MoLDS across hyperparameters on the PMd training split and select the model by validation criteria (NLL/RMSE/BIC). Figure 5(a) reports validation results, and Fig. 5(b) shows test one-step-ahead reconstructions.

To accommodate continuously distributed reach angles, trials are uniformly binned on the circle (12 bins). Within each bin, the dominant component is the one with the largest mean responsibility. Figure 5(c) colors bins by their dominant LDS component and overlays responsibility-weighted preferred-direction (PD) arrows for each component. Figure 5(d) plots impulse-response magnitudes versus lag of each component, revealing component-specific gains and temporal decay (Appendix D.2, Fig. 7, further decomposes input-channel responses). Component usage fractions on held-out test trials are shown in Fig. 5(e). Overall, the mixture components specialize in distinct movement directions and exhibit distinct dynamical response profiles.

6 CONCLUSION

MoLDS offers an interpretable way to model repeated, trajectory-level dynamics in heterogeneous neural recordings. Here, we propose a Tensor-EM algorithm for inference of MoLDS; we use SMD for tensor decomposition as an initialization with Kalman filter-smoother EM, to achieve reliable parameter recovery and interpretable clustering of synthetic and real neural recordings. This hybrid framework makes MoLDS practically usable for large, noisy datasets. As limitations, we note that we have only explored synthetic and real-world cases where the data is likely to have linear dynamics - the synthetic data is linear and the neural data consists of smoothed firing rates - and have not explored cases with high likelihood of model mismatch. Regardless, this study sets the stage for broader applications of MoLDS to complex systems.

7 ETHICS STATEMENT

Here, we aim to make methodological and neuroscientific insights, and do not note any negative societal or ethical implications.

8 REPRODUCIBILITY STATEMENT

Our work can be reproduced in a straightforward way. The datasets are provided in Miller (2022) and Perich et al. (2018), with all pre-processing techniques detailed in Chowdhury et al. (2020), Lawlor et al. (2018a), and the Appendix. Moreover, detailed algorithms and technical details are provided for each step of the inference, with comprehensive pseudo-code for the implementation in the main text and Appendix.

REFERENCES

- Animashree Anandkumar, Rong Ge, Daniel J Hsu, Sham M Kakade, Matus Telgarsky, et al. Tensor decompositions for learning latent variable models. *J. Mach. Learn. Res.*, 15(1):2773–2832, 2014.
- Ainesh Bakshi, Allen Liu, Ankur Moitra, and Morris Yau. Tensor decompositions meet control theory: learning general mixtures of linear dynamical systems. In *International Conference on Machine Learning*, pp. 1549–1563. PMLR, 2023.
- Christopher M Bishop. *Pattern recognition and machine learning*, volume 4. Springer, 2006.
- Hengnu Chen, Lei Deng, Zheng Qu, Ling Liang, Tianyi Yan, Yuan Xie, and Guoqi Li. Tensor train decomposition for solving large-scale linear equations. *Neurocomputing*, 464:203–217, 2021.
- Yanxi Chen and H Vincent Poor. Learning mixtures of linear dynamical systems. In *International conference on machine learning*, pp. 3507–3557. PMLR, 2022.
- Raeed H Chowdhury, Joshua I Glaser, and Lee E Miller. Area 2 of primary somatosensory cortex encodes kinematics of the whole arm. *Elife*, 9:e48198, 2020.
- Richard D De Veaux. Mixtures of linear regressions. *Computational Statistics & Data Analysis*, 8(3): 227–245, 1989.
- Arthur P Dempster, Nan M Laird, and Donald B Rubin. Maximum likelihood from incomplete data via the em algorithm. *Journal of the royal statistical society: series B*, 39(1):1–22, 1977.
- James Durbin and Siem Jan Koopman. *Time series analysis by state space methods*. Oxford university press, 2012.
- Emily Beth Fox. *Bayesian nonparametric learning of complex dynamical phenomena*. PhD thesis, Massachusetts Institute of Technology, 2009.
- Zoubin Ghahramani and Geoffrey E Hinton. Parameter estimation for linear dynamical systems. 1996.

- Zoubin Ghahramani and Geoffrey E Hinton. Variational learning for switching state-space models. *Neural computation*, 12(4):831–864, 2000.
- Volodymyr Kuleshov, Arun Chaganty, and Percy Liang. Tensor factorization via matrix factorization. In *Artificial Intelligence and Statistics*, pp. 507–516. PMLR, 2015.
- Patrick N. Lawlor, Matthew G. Perich, Lee E. Miller, and Konrad P. Kording. Linear-nonlinear-time-warp-poisson models of neural activity. *Journal of Computational Neuroscience*, 45(3):173–191, October 2018a. ISSN 1573-6873.
- Patrick N Lawlor, Matthew G Perich, Lee E Miller, and Konrad P Kording. Linear-nonlinear-time-warp-poisson models of neural activity. *Journal of computational neuroscience*, 45(3):173–191, 2018b.
- Yuanzhi Li and Yingyu Liang. Learning mixtures of linear regressions with nearly optimal complexity. In *Conference On Learning Theory*, pp. 1125–1144. PMLR, 2018.
- Scott Linderman, Matthew Johnson, Andrew Miller, Ryan Adams, David Blei, and Liam Paninski. Bayesian learning and inference in recurrent switching linear dynamical systems. In *Artificial intelligence and statistics*, pp. 914–922. PMLR, 2017.
- Lennart Ljung. System identification. In *Signal analysis and prediction*, pp. 163–173. Springer, 1998.
- Lee Miller. Area2 bump: macaque somatosensory area 2 spiking activity during reaching with perturbations, 2022. URL <https://dandiarchive.org/dandiset/000127/0.220113.0359>.
- Samet Oymak and Necmiye Ozay. Non-asymptotic identification of lti systems from a single trajectory. In *2019 American control conference (ACC)*, pp. 5655–5661. IEEE, 2019.
- Soumyabrata Pal, Arya Mazumdar, Rajat Sen, and Avishek Ghosh. On learning mixture of linear regressions in the non-realizable setting. In *International Conference on Machine Learning*, pp. 17202–17220. PMLR, 2022.
- Liam Paninski and John P Cunningham. Neural data science: accelerating the experiment-analysis-theory cycle in large-scale neuroscience. *Current opinion in neurobiology*, 50:232–241, 2018.
- Matthew G. Perich, Patrick N. Lawlor, Konrad P. Kording, and Lee E. Miller. Extracellular neural recordings from macaque primary and dorsal premotor motor cortex during a sequential reaching task, 2018. URL <http://crcns.org/data-sets/motor-cortex/pmd-1>.
- Maryann Rui and Munther Dahleh. Finite sample analysis of tensor decomposition for learning mixtures of linear systems. In *7th Annual Learning for Dynamics & Control Conference*, pp. 1313–1325. PMLR, 2025.
- Carsen Stringer and Marius Pachitariu. Analysis methods for large-scale neuronal recordings. *Science*, 386(6722):eadp7429, 2024.
- Anne E Urai, Brent Doiron, Andrew M Leifer, and Anne K Churchland. Large-scale neural recordings call for new insights to link brain and behavior. *Nature neuroscience*, 25(1):11–19, 2022.
- Xinyang Yi, Constantine Caramanis, and Sujay Sanghavi. Solving a mixture of many random linear equations by tensor decomposition and alternating minimization. *arXiv preprint arXiv:1608.05749*, 2016.
- Kai Zhong, Prateek Jain, and Inderjit S Dhillon. Mixed linear regression with multiple components. *Advances in neural information processing systems*, 29, 2016.

A TENSOR INITIALIZATION DETAILS

In this section, we provide a brief introduction to MoLDS's connection to MLR and the tensor-based moment method for MoLDS (see Bakshi et al. (2023); Rui & Dahleh (2025) for more details).

A.1 MoLDS TO MLR REFORMULATION

The key insight enabling tensor methods for MoLDS is that any linear dynamical system can be equivalently represented through its *impulse response* (also called Markov parameters), which describe how the system responds to unit impulses in its inputs. This representation allows us to reformulate MoLDS as MLR, making algebraic moment-based methods applicable.

Step 1: Impulse response representation. For notational brevity, we assume an LDS with m -dimensional inputs and a scalar output ($p = 1$), and zero feedthrough ($D_k = 0$). The extension to multiple outputs ($p > 1$) is straightforward. The system parameters are (A_k, B_k, C_k) . Its impulse response, also called the sequence of Markov parameters, is defined by

$$g_k(j) = C_k A_k^{j-1} B_k \in \mathbb{R}^m, \quad j = 1, 2, 3, \dots, \quad (7)$$

so that $g_k(1) = C_k B_k$, $g_k(2) = C_k A_k B_k$, etc.

The sequence $\{g_k(j)\}$ captures the system's memory: $g_k(j)$ specifies how an input applied j steps in the past influences the current output. Given an input sequence $\{u_t\}$, the output can be expressed as the infinite convolution

$$y_t = \sum_{j=1}^{\infty} g_k(j) u_{t-j} + \text{noise terms}. \quad (8)$$

In practice, this sum is truncated after L terms, since $g_k(j)$ decays exponentially for stable systems. We denote the stacked first L impulse responses by

$$g_k^{(L)} = [g_k(1)^\top, g_k(2)^\top, \dots, g_k(L)^\top]^\top \in \mathbb{R}^{Lm}. \quad (9)$$

Step 2: Lagged input construction. To exploit the impulse response representation, we construct *lagged input vectors* that collect recent input history. For trajectory i at time $t \geq L$, define

$$\bar{u}_{i,t} = [u_{i,t}^\top, u_{i,t-1}^\top, \dots, u_{i,t-L+1}^\top]^\top \in \mathbb{R}^{Lm}. \quad (10)$$

This vector stacks the most recent L inputs (the current input and the previous $L - 1$), so that $\bar{u}_{i,t}$ has dimension Lm and aligns with the stacked impulse responses $g_k^{(L)}$. With this construction, the truncated output becomes

$$y_{i,t} \approx \langle g_{k_i}^{(L)}, \bar{u}_{i,t} \rangle + \text{noise terms}, \quad (11)$$

where k_i denotes the (unknown) component generating trajectory i .

With the above input construction, consecutive lagged vectors $\bar{u}_{i,t}$ and $\bar{u}_{i,t+1}$ share $L - 1$ input entries, which induces strong statistical dependence and complicates the estimation of higher-order moments. To mitigate this, we sub-sample the time indices with a stride L , i.e.,

$$t \in \{L, 2L, 3L, \dots, T\}.$$

This construction ensures that the resulting lagged vectors are non-overlapping. Under standard input assumptions (e.g., i.i.d. or persistently exciting inputs), the sub-sampled vectors are approximately independent, which is crucial for consistent moment estimation.

Step 3: Normalization and MLR formulation. To apply tensor methods, the covariates must have unit variance. We therefore normalize each lagged input by the input standard deviation,

$$v_j = \frac{\bar{u}_{i,t}}{\sigma_u}, \quad \sigma_u^2 = \mathbb{E}[\|u_t\|^2],$$

and flatten the dataset via the re-indexing map $(i, t) \mapsto j$. This yields the mixture of linear regressions (MLR) form

$$\tilde{y}_j = \langle v_j, \beta_{k_j} \rangle + \eta_j + \xi_j, \quad (12)$$

where

- $\tilde{y}_j = y_{i,t}$ is the observed output,
- $v_j \in \mathbb{R}^{Lm}$ is the normalized lagged input (covariate),
- $\beta_{k_j} = \sigma_u g_{k_j}^{(L)} \in \mathbb{R}^{Lm}$ is the scaled Markov parameter vector (regression coefficient),
- $k_j \in \{1, \dots, K\}$ is the (unknown) component index,
- η_j captures process and observation noise,
- ξ_j accounts for truncation error from ignoring impulse responses beyond lag L .

Step 4: Mixture structure. Since each trajectory originates from one of K latent LDS components with probabilities $\{p_k\}_{k=1}^K$, the regression model inherits the same mixture structure:

$$\mathbb{P}[k_j = k] = p_k.$$

Thus the learning task reduces to recovering the mixture weights $\{p_k\}$ and regression vectors $\{\beta_k\}$ from the dataset $\{(v_j, \tilde{y}_j)\}$. Once these regression parameters are estimated, the corresponding state-space models (A_k, B_k, C_k) can be reconstructed via the Ho–Kalman realization algorithm Oymak & Ozay (2019).

This reformulation is crucial: it transforms the original problem of identifying a mixture of LDSs into the algebraic problem of learning an MLR model, for which polynomial-time tensor methods with identifiability and sample-complexity guarantees are available Rui & Dahleh (2025).

A.2 MOMENT CONSTRUCTION AND WHITENING

Let $d = Lm$ denote the dimension of the lagged input vectors. We partition the sample indices into two disjoint subsets \mathcal{N}_2 and \mathcal{N}_3 for constructing second- and third-order moments, respectively. The empirical moments are defined as

$$M_2 = \frac{1}{2|\mathcal{N}_2|} \sum_{j \in \mathcal{N}_2} \tilde{y}_j^2 (v_j \otimes v_j - I_d), \quad M_3 = \frac{1}{6|\mathcal{N}_3|} \sum_{j \in \mathcal{N}_3} \tilde{y}_j^3 (v_j^{\otimes 3} - \mathcal{E}(v_j)), \quad (13)$$

where I_d is the $d \times d$ identity and

$$\mathcal{E}(v) = \sum_{r=1}^d (v \otimes e_r \otimes e_r + e_r \otimes v \otimes e_r + e_r \otimes e_r \otimes v),$$

with e_r the r -th standard basis vector in \mathbb{R}^d . These corrections ensure that the resulting tensors are centered and symmetric.

At the population level, these moments satisfy

$$\mathbb{E}[M_2] = \sum_{k=1}^K p_k \beta_k \beta_k^\top, \quad \mathbb{E}[M_3] = \sum_{k=1}^K p_k \beta_k^{\otimes 3}, \quad (14)$$

so they encode the regression vectors $\{\beta_k\}$ and mixture weights $\{p_k\}$.

To obtain an orthogonally decomposable form, we perform whitening. Let $M_2 \approx U \Sigma U^\top$ be the rank- K eigendecomposition, and define

$$W = U(:, 1:K) \Sigma_{1:K}^{-1/2}, \quad (15)$$

so that $W^\top M_2 W \approx I_K$. Applying W along each mode of M_3 yields the whitened tensor

$$\hat{T} = M_3(W, W, W) = \sum_{k=1}^K p_k \alpha_k^{\otimes 3}, \quad \alpha_k := W^\top \beta_k. \quad (16)$$

This tensor is symmetric and orthogonally decomposable. We then apply Simultaneous Matrix Diagonalization (SMD) (A.3) to recover $\{\alpha_k, p_k\}$. Finally, we unwhiten to obtain $\beta_k = W^{-\top} \alpha_k$, and recover the state-space parameters (A_k, B_k, C_k) via Ho–Kalman realization Oymak & Ozay (2019).

A.3 SIMULTANEOUS MATRIX DIAGONALIZATION

This section provides the Simultaneous Matrix Diagonalization (SMD) method for tensor decomposition Kuleshov et al. (2015) in Algorithm 2. SMD recovers tensor components by reducing the problem to joint matrix diagonalization, exploiting linear-algebraic structure to recover all components simultaneously rather than sequentially as in RTPM.

Algorithm 2 Simultaneous Matrix Diagonalization (SMD) for Tensor Decomposition

Require: Noisy symmetric tensor $\widehat{T} \in \mathbb{R}^{K \times K \times K}$; number of random probes $L_0 \geq 2$.

Ensure: Factor estimates $\{\hat{\alpha}_i\}_{i=1}^K$ and weights $\{\hat{p}_i\}_{i=1}^K$ such that $\widehat{T} \approx \sum_{i=1}^K \hat{p}_i \hat{\alpha}_i^{\otimes 3}$.

Stage 1: random projections → simultaneous diagonalization

- 1: Sample $\{w_\ell\}_{\ell=1}^{L_0}$ i.i.d. from the unit sphere \mathbb{S}^{K-1} .
- 2: Form projected matrices $\mathcal{M}^{(0)} \leftarrow \{\widehat{T}(I, I, w_\ell)\}_{\ell=1}^{L_0}$, where $\widehat{T}(I, I, w) = \sum_{r=1}^K w_r \widehat{T}(:, :, r)$.
- 3: Compute an approximate joint diagonalizer via **JJD**: $U^{(0)} \leftarrow \text{JJD}(\mathcal{M}^{(0)})$.
- 4: Set $V^{(0)} \leftarrow (U^{(0)})^{-1}$.

Stage 2: inverse-guided projections → refinement

- 5: Build $\mathcal{M}^{(1)} \leftarrow \{\widehat{T}(I, I, v_i^{(0)})\}_{i=1}^K$, where $v_i^{(0)}$ is the i -th column of $V^{(0)}$.
 - 6: Refine with **JJD**: $U^{(1)} \leftarrow \text{JJD}(\mathcal{M}^{(1)})$.
 - 7: Let $\hat{\alpha}_i$ be the i -th column of $U^{(1)}$ and normalize to $\|\hat{\alpha}_i\|_2 = 1$.
 - 8: **for** $i = 1$ to K **do**
 - 9: $\hat{p}_i \leftarrow \langle \widehat{T}, \hat{\alpha}_i \otimes \hat{\alpha}_i \otimes \hat{\alpha}_i \rangle$.
 - 10: **end for**
 - 11: **return** $\{\hat{\alpha}_i\}_{i=1}^K, \{\hat{p}_i\}_{i=1}^K$.
-

Jacobi Joint Diagonalization (JJD). Given matrices $\{M_\ell\}_{\ell=1}^{L_0}$, JJD finds an orthogonal matrix U such that $U^\top M_\ell U$ is as close to diagonal as possible for all ℓ simultaneously. We use the Jacobi rotation-based algorithm that iteratively applies Givens rotations to minimize the off-diagonal Frobenius norm $\sum_\ell \|U^\top M_\ell U - \text{diag}(U^\top M_\ell U)\|_F^2$. Convergence is declared when the relative change in this objective falls below 10^{-8} .

A.4 TENSOR INITIALIZATION ALGORITHM

With the MLR reformulation and SMD tensor method, the full algorithm of tensor initialization for MoLDS is provided below.

Algorithm 3 Tensor Initialization for MoLDS

Require: Trajectories $\{(u_{i,0:T_i-1}, y_{i,0:T_i-1})\}_{i=1}^N$, truncation L , LDS order n , #components K

Ensure: Estimates of mixture weights $\hat{p}_{1:K}$ and LDS params $\{(\hat{A}_k, \hat{B}_k, \hat{C}_k, \hat{D}_k)\}_{k=1}^K$

(A) MoLDS → MLR design & sub-sampling

- 1: **for** $i = 1:N$ **do**
 - 2: **for** $t \in \{L, 2L, \dots, T_i\}$ **do**
 - 3: $\bar{u}_{i,t} \leftarrow [u_{i,t}^\top, u_{i,t-1}^\top, \dots, u_{i,t-L+1}^\top]^\top \in \mathbb{R}^{Lm}$
 - 4: Append sample (v_j, \tilde{y}_j) with $v_j \leftarrow \bar{u}_{i,t}/\sigma_u$, $\tilde{y}_j \leftarrow y_{i,t}$
 - 5: **end for**
 - 6: **end for**
 - 7: Partition samples: $\{1, \dots, M\} = \mathcal{N}_2 \dot{\cup} \mathcal{N}_3$ where $M = \sum_i |T_i|/L$
 - 8: **(B) Moment construction**
 - 9: $M_2 \leftarrow \frac{1}{2|\mathcal{N}_2|} \sum_{j \in \mathcal{N}_2} \tilde{y}_j^2 (v_j \otimes v_j - I_d)$
 - 10: $M_3 \leftarrow \frac{1}{6|\mathcal{N}_3|} \sum_{j \in \mathcal{N}_3} \tilde{y}_j^3 (v_j \otimes v_j \otimes v_j - \mathcal{E}(v_j))$ where $d = Lm$
 - 11: **(C) Symmetric whitening and tensor formation**
 - 12: Compute rank- K SVD: $M_2 \approx U \Sigma U^\top$, set $W \leftarrow U_{(:,1:K)} \Sigma_{1:K}^{-1/2}$
 - 13: Form whitened tensor: $\hat{T} \leftarrow M_3(W, W, W) \in \mathbb{R}^{K \times K \times K}$
 - 14: **(D) Tensor decomposition & recovery**
 - 15: Apply SMD to \hat{T} to recover $\{\hat{\alpha}_k, \hat{p}_k\}_{k=1}^K$ (Appendix Alg 2)
 - 16: Unwhiten: $\hat{\beta}_k \leftarrow W^{-\top} \hat{\alpha}_k$ and recover Markov params $\hat{g}_k^{(L)} \leftarrow \hat{\beta}_k/\sigma_u$
 - 17: **(E) State-space realization**
 - 18: **for** $k = 1:K$ **do**
 - 19: Build Hankel matrix from $\{\hat{g}_k^{(h)}\}_{h=1}^L$ and apply Ho–Kalman algorithm
 - 20: Recover state-space parameters $(\hat{A}_k, \hat{B}_k, \hat{C}_k, \hat{D}_k)$
 - 21: **end for**
 - 22: **return** $\{\hat{p}_k\}_{k=1}^K$ and $\{(\hat{A}_k, \hat{B}_k, \hat{C}_k, \hat{D}_k)\}_{k=1}^K$
-

Under standard identifiability and excitation conditions, RTPM-based tensor decomposition provably recovers the parameters $\{\beta_k\}$ with finite-sample guarantees Rui & Dahleh (2025). Simultaneous matrix diagonalization (SMD) enjoys analogous guarantees in the orthogonal-tensor setting and, in practice, tends to be more numerically stable and noise-robust Kuleshov et al. (2015). These advantages lead to improved parameter estimates during the tensor initialization stage (Figure 1, main paper), which in turn can provide a stronger starting point for the subsequent EM refinement.

B EM FOR MoLDS: COMPLETE TECHNICAL DETAILS

B.1 OVERVIEW AND STRUCTURE

This appendix provides complete technical details for our EM formulation for MoLDS. The EM algorithm for MoLDS alternates between two phases: (i) an E-step that computes trajectory-wise responsibilities via Kalman filter likelihoods and extracts sufficient statistics via Kalman smoothing, and (ii) an M-step that updates all parameters using closed-form maximum likelihood estimates from responsibility-weighted statistics. The algorithm is detailed in Algorithm 4.

B.2 COMPLETE EM ALGORITHM

The EM procedure operates on trajectories $\{(u_{i,0:T_i-1}, y_{i,0:T_i-1})\}_{i=1}^N$ with current parameter estimates $\hat{\theta}^{(t)} = \{(\hat{p}_k, \hat{A}_k, \hat{B}_k, \hat{C}_k, \hat{D}_k, \hat{Q}_k, \hat{R}_k)\}_{k=1}^K$ at iteration t .

E-step Computations. For each trajectory i and component k , we compute:

$$\ell_{i,k} = \log p(y_{i,0:T_i-1} | u_{i,0:T_i-1}, \hat{\theta}_k^{(t)}), \quad (17)$$

$$\alpha_{i,k} = \log \hat{p}_k^{(t)} + \ell_{i,k}, \quad (18)$$

$$\gamma_{i,k} = \frac{\exp(\alpha_{i,k})}{\sum_{r=1}^K \exp(\alpha_{i,r})}, \quad \sum_{k=1}^K \gamma_{i,k} = 1. \quad (19)$$

The likelihood $\ell_{i,k}$ is computed via the Kalman filter, while responsibilities $\gamma_{i,k}$ use the log-sum-exp trick for numerical stability. Subsequently, the Kalman smoother computes per-trajectory sufficient statistics $S_{i,k}$, which are aggregated as:

$$S_k = \sum_{i=1}^N \gamma_{i,k} S_{i,k}. \quad (20)$$

M-step Updates. Mixture weights and LDS parameters are updated via:

$$\hat{p}_k^{(t+1)} = \frac{1}{N} \sum_{i=1}^N \gamma_{i,k}, \quad (21)$$

$$\hat{\theta}_k^{(t+1)} = \text{MLE-LDS}(S_k), \quad (22)$$

where the closed-form LDS parameter updates are derived in B.3.

Convergence. The algorithm monitors the observed-data log-likelihood:

$$\mathcal{L}^{(t+1)} = \sum_{i=1}^N \log \sum_{k=1}^K \hat{p}_k^{(t+1)} p(y_{i,0:T_i-1} | u_{i,0:T_i-1}, \hat{\theta}_k^{(t+1)}), \quad (23)$$

and terminates when the relative improvement falls below the threshold ε .

Algorithm 4 EM Refinement for MoLDS

Require: Trajectories $\{(u_{i,0:T_i-1}, y_{i,0:T_i-1})\}_{i=1}^N$; initial parameters $\hat{\theta}^{(0)}$; max iterations EM_max; tolerance ε

Ensure: Refined mixture weights and LDS parameters

- 1: **for** iter = 1 to EM_max **do**
- E-step: Compute responsibilities and sufficient statistics**
- 2: **for** $i = 1 : N$ **do**
- 3: **for** $k = 1 : K$ **do**
- 4: Compute $\ell_{i,k}$ via Kalman filter on $(u_{i,0:T_i-1}, y_{i,0:T_i-1})$ using $\hat{\theta}_k^{(\text{iter}-1)}$
- 5: Set $\alpha_{i,k} \leftarrow \log \hat{p}_k^{(\text{iter}-1)} + \ell_{i,k}$
- 6: Run Kalman smoother to compute sufficient statistics $S_{i,k}$
- 7: **end for**
- 8: Compute $\text{lse}_i \leftarrow \log \sum_{r=1}^K \exp(\alpha_{i,r})$ and responsibilities $\gamma_{i,k} \leftarrow \exp(\alpha_{i,k} - \text{lse}_i)$
- 9: **end for**
- 10: Aggregate responsibility-weighted statistics: $S_k \leftarrow \sum_{i=1}^N \gamma_{i,k} S_{i,k}$ for each k
- M-step: Update all parameters**
- 11: Update mixture weights: $\hat{p}_k^{(\text{iter})} \leftarrow \frac{1}{N} \sum_{i=1}^N \gamma_{i,k}$ for all k
- 12: **for** $k = 1 : K$ **do**
- 13: Update LDS parameters $(\hat{A}_k, \hat{B}_k, \hat{C}_k, \hat{D}_k, \hat{Q}_k, \hat{R}_k)$ from S_k (see B.3)
- 14: **end for**
- Convergence check**
- 15: Compute observed log-likelihood: $\mathcal{L}^{(\text{iter})} \leftarrow \sum_{i=1}^N \text{lse}_i$
- 16: **Stop if** $(\mathcal{L}^{(\text{iter})} - \mathcal{L}^{(\text{iter}-1)}) / |\mathcal{L}^{(\text{iter}-1)}| < \varepsilon$
- 17: **end for**
- 18: **Return** $\{\hat{p}_k, (\hat{A}_k, \hat{B}_k, \hat{C}_k, \hat{D}_k, \hat{Q}_k, \hat{R}_k)\}_{k=1}^K$

B.3 CLOSED-FORM M-STEP UPDATES

The M-step updates follow standard LDS maximum likelihood estimation Ghahramani & Hinton (1996). For simplicity, we present the case $D_k = 0$ (no direct feedthrough) and drop component and iteration indices (k, t) for readability:

We solve the normal equations with optional ridge regularization $\lambda > 0$ to obtain system matrices for each component.

$$[A \quad B] = [S_{xx^-} \quad S_{xu^-}] \left(\begin{bmatrix} S_{x-x^-} & S_{u^-x^-}^\top \\ S_{u^-x^-} & S_{u^-u^-} \end{bmatrix} + \lambda I \right)^{-1}, \quad (24)$$

$$C = S_{yx} (S_{xx} + \lambda I)^{-1}. \quad (25)$$

And the noise covariances are

$$\begin{aligned} R &= \frac{1}{T} (S_{yy} - CS_{yx}^\top - S_{yx}C^\top + CS_{xx}C^\top), \\ Q &= \frac{1}{N} \left(S_{xx,\text{curr}} - AS_{xx^-}^\top - BS_{xu^-}^\top - (AS_{xx^-}^\top + BS_{xu^-}^\top)^\top \right. \\ &\quad \left. + AS_{x-x^-} A^\top + AS_{u^-x^-}^\top B^\top + BS_{u^-x^-} A^\top + BS_{u^-u^-} B^\top \right). \end{aligned}$$

Here, all $S_{\cdot,\cdot}$ are the sufficient statistics.

B.4 COMPUTATIONAL COMPLEXITY

Each EM iteration requires $O(NKn^3T)$ operations:

- Kalman filtering: $O(n^3T)$ per trajectory-component pair, total $O(NKn^3T)$
- Kalman smoothing: $O(n^3T)$ per trajectory-component pair, total $O(NKn^3T)$
- M-step updates: $O(Kn^3)$ for matrix inversions

Tensor initialization significantly reduces the iteration count compared to random initialization, which substantially improves computational efficiency. The tensor initialization phase requires $O(d^3)$ operations where $d = Lm$ is the MLR dimension, making it negligible in the whole Tensor-EM pipeline.

C INITIALIZING (Q, R) AFTER TENSOR INITIALIZATION

The tensor stage yields $\{\hat{A}_z, \hat{B}_z, \hat{C}_z, \hat{p}_z\}_{z=1}^K$ but not the noise covariances $\{\hat{Q}_z, \hat{R}_z\}$. We initialize (Q_z, R_z) from data for each component z as follows.

Step 1 (labels/weights; optional). Assign labels by selecting, for each trajectory i , the component z with the smallest one-step prediction MSE under $(\hat{A}_z, \hat{B}_z, \hat{C}_z)$, and set $w_{i,z} = 1$ for that component and $w_{i,r} = 0$ for all $r \neq z$.

Step 2 (state back-projection). For each z and trajectory i , decode provisional latents with a ridge pseudo-inverse:

$$\hat{x}_{i,t}^{(z)} = (\hat{C}_z^\top \hat{C}_z + \lambda I)^{-1} \hat{C}_z^\top (y_{i,t} - \hat{D}_z u_{i,t}),$$

where we use $\lambda = 10^{-6} \max(\text{diag}(\hat{C}_z^\top \hat{C}_z))$ for numerical stability.

Step 3 (residual covariances). Define

$$\eta_{i,t}^{(z)} = \hat{x}_{i,t+1}^{(z)} - \hat{A}_z \hat{x}_{i,t}^{(z)} - \hat{B}_z u_{i,t}, \quad \varepsilon_{i,t}^{(z)} = y_{i,t} - \hat{C}_z \hat{x}_{i,t}^{(z)} - \hat{D}_z u_{i,t}.$$

With $T_i^{\text{tr}} = T_i - 1$, we set

$$\hat{Q}_z^{(0)} = \frac{\sum_i w_{i,z} \sum_{t=0}^{T_i-2} \eta_{i,t}^{(z)} \eta_{i,t}^{(z)\top}}{\sum_i w_{i,z} T_i^{\text{tr}}}, \quad \hat{R}_z^{(0)} = \frac{\sum_i w_{i,z} \sum_{t=0}^{T_i-1} \varepsilon_{i,t}^{(z)} \varepsilon_{i,t}^{(z)\top}}{\sum_i w_{i,z} T_i}. \quad (26)$$

Step 4 (positive semidefinite projection). Symmetrize and project to the positive semidefinite cone:

$$\hat{Q}_z^{(0)} \leftarrow \Pi_{\geq 0}\left(\frac{1}{2}(\hat{Q}_z^{(0)} + \hat{Q}_z^{(0)\top})\right), \quad \hat{R}_z^{(0)} \leftarrow \Pi_{\geq 0}\left(\frac{1}{2}(\hat{R}_z^{(0)} + \hat{R}_z^{(0)\top})\right),$$

where $\Pi_{\geq 0}(M)$ projects matrix M to the nearest positive semidefinite matrix via eigendecomposition: if $M = U\Lambda U^\top$, then $\Pi_{\geq 0}(M) = U \max(\Lambda, 0) U^\top$.

This yields $(\hat{Q}_z^{(0)}, \hat{R}_z^{(0)})$ for each component z , providing a stable initialization for the first E-step; subsequent EM iterations refine (Q_z, R_z) from responsibility-weighted sufficient statistics.

D TENSOR-EM MoLDS APPLICATION ON NEURAL DATASET DETAILS

D.1 AREA2 DATASET

Dataset introduction. We evaluate our methods on a neural population dataset recorded from the motor cortex (Area2) of a rhesus macaque. The task is a center-out reaching paradigm where the subject applies force to a manipulandum in response to cues. Neural activity was recorded with a Utah array and spike counts were extracted from thresholded multiunit activity. The dataset provides simultaneously measured behavioral covariates (applied force, hand kinematics) alongside the neural recordings.

Data preparation for MoLDS. Following the Neural Latents Benchmark preprocessing, we first apply principal component analysis (PCA) to reduce the neural activity to p latent dimensions (here $p = 6$). The behavioral force signals (6D) are used as exogenous inputs. For MoLDS training, we constructed input-output trials of the form (u_t, y_t) , where $u_t \in \mathbb{R}^6$ corresponds to force inputs and $y_t \in \mathbb{R}^p$ are PCA-reduced neural outputs. Each reaching direction corresponds to a separate trial. We split the dataset into non-overlapping `train`, `val`, and `test` sets, ensuring balanced coverage across each direction.

Tensor-EM MoLDS train/val/test setup. For model initialization, we computed input-output moment tensors from the training data and applied Simultaneous Matrix Diagonalization (SMD) to obtain globally consistent estimates of system parameters and mixture weights. These estimates were used to initialize a full Kalman filter-smoother EM refinement, which updates all LDS parameters in closed form. We trained MoLDS models with different numbers of mixture components $K \in \{3, 4, 5\}$, latent dimension $n \in \{3, 4, 5\}$, and lag parameters $L \in \{16, 24\}$. Validation data is used for model selection by comparing negative log-likelihood (NLL), root mean squared error (RMSE), and Bayesian Information Criterion (BIC).

- **NLL:** sum of Gaussian-innovation log-likelihoods.
- **RMSE:** root mean squared error of one-step predictions \hat{y}_t vs. y_t .
- **BIC:** $BIC = -2 \text{NLL} + p_\theta \log N_{\text{obs}}$, where p_θ is the total parameter count and N_{obs} the number of observed outputs.

The best configuration was tested on the held-out `test` set.

Per-trial responsibilities. We compute responsibilities for each trial under component k

$$r_{ik} \propto \exp(\ell_k^{(i)}), \quad \sum_{k=1}^K r_{ik} = 1, \tag{27}$$

where $\ell_k^{(i)}$ is the one-step Kalman log-likelihood of trial i under component k . Global usage is summarized by $\text{usage}_k = \frac{1}{N} \sum_i r_{ik}$.

Analysis.

1. **Validation metrics.** We plot BIC/NLL/RMSE across K and initializations (Tensor vs. Random) to assess stability and choose capacity.

2. **Representative predictions.** We visualize \hat{y}_t vs. y_t for representative test trials (all p outputs).
3. **Direction organization & component usage.** In a polar wheel with one wedge per discrete direction, we color each wedge by the dominant component (highest mean r_{ik} among trials in that wedge).
4. **Markov response comparison.** For each component, we calculate $g_k(\tau) = C_k A_k^\tau B_k \in \mathbb{R}^{p \times m}$, $\tau = 0, \dots, L - 1$ (omit D_k for clarity). Plot $\|g_k(\tau)\|_F$ for all components on a single axis to compare gain/decay.
5. **Global geometry of dynamics.** Vectorize all $\{g_k(\tau)\}_{k,\tau}$, run PCA across that set, and scatter the first two PCs; use color to encode lag τ and marker/edge to encode component. Components typically form distinct, smoothly evolving trajectories.

Supervised per-direction baseline. Because Area2 uses *discrete* directions, we also fit a single LDS per direction using the same observation space. We compute each supervised model’s impulse response, cluster the per-direction vectors, and align clusters to MoLDS components via a Hungarian assignment on centroid distances. A polar plot (inner = supervised clusters, outer = MoLDS predictions) confirms that unsupervised MoLDS recovers direction-consistent dynamics.

SLDS comparison. We fit switching LDS (SLDS) models with $S \in 1, 2, 3$ discrete states to the training set (Gaussian emissions, 6-D force inputs, sticky transitions). Validation NLL/BIC selected $S = 2$ SLDS. We then decoded the test set with Viterbi and summarized the inferred state sequences (Fig. 6). Panel (a) shows that within-trial switches are infrequent and tend to occur in similar temporal regions across trials. In panel (b, left), grouping test trials by their dominant state s^* reveals that the same state dominates most directions, with only a mild departure around dir-90. The mean time-share view (b, right) tells the same story: state composition looks broadly similar across directions. Consistent with this, a “collapsed” SLDS that uses only each trial’s dominant state achieves nearly the same predictive metrics as the fully segmented model, indicating that within-trial switching adds little in this dataset. These results support our interpretation that the primary structure is between trials (by direction), not within trials.

D.2 PMD DATASET

Dataset introduction. The dorsal premotor cortex (PMd) dataset contains single-trial reaches, where time-aligned kinematics (position/velocity/acceleration) and multi-unit spikes, plus a reach direction angle $\theta \in (-\pi, \pi]$ are stored. For MoLDS, the input and observation are taken as

$$U_t = [v_x, v_y, a_x, a_y, \text{speed}] \in \mathbb{R}^5, \quad Y_t \in \mathbb{R}^{16},$$

where speed = $\sqrt{v_x^2 + v_y^2}$ and Y_t denotes PCA-reduced, z -scored firing rates. As in Area2 (App. D.1), angles are used only for analysis/visualization; MoLDS is trained without angle labels.

Tensor-EM MoLDS train/val/test setup. Training and selection mirror Area2: tensor or random initialization followed by EM refinement; Model selection was performed on the validation split. For PMd, we sweep $K \in \{2, 3, 4\}$, $n \in \{4, 5, 6\}$, and Markov horizon $L \in \{12, 16, 24\}$. The selected model in our experiments is $K=4$, $n=5$, $L=12$.

Analysis. We reuse the analysis logic from Area2. As the direction angles are not discrete as in Area2, we split them into 12 bins, and each bin is colored by the dominant component (largest mean r_{ik} in the bin). Component-wise preferred directions are shown by responsibility-weighted arrows

$$v_k = \sum_i r_{ik} [\cos \theta_i, \sin \theta_i],$$

plotted as an inset (angle $\angle v_k$, length $\|v_k\|$). For each component, we examine the Markov parameter blocks

$$g_k(\tau) = C_k A_k^\tau B_k \in \mathbb{R}^{p \times m}, \quad \tau = 0, \dots, L - 1,$$

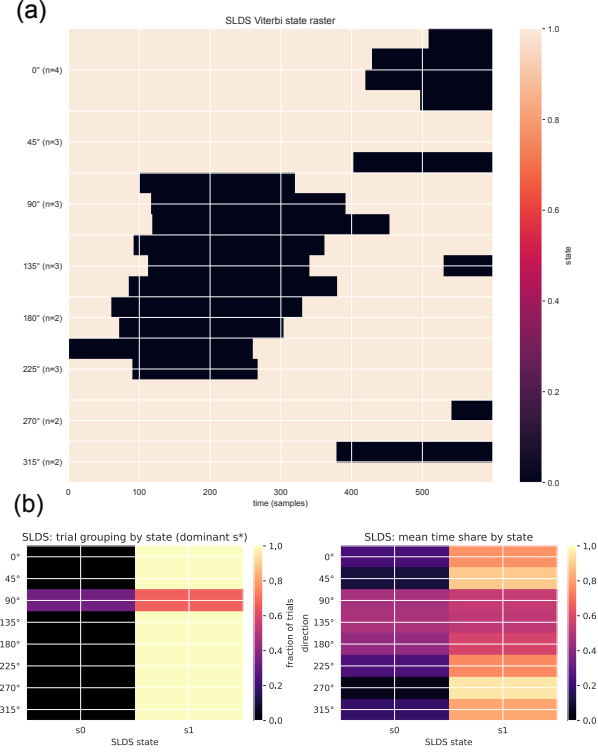


Figure 6: **SLDS result:** (a) Inferred switch states for all test trials. (b) Group trials and mean time by states.

and plot (a) the compact magnitude curves $\|g_k(\tau)\|_F$ and (b) per-input energies $E_{k,j}(\tau) = \|g_k(\tau)_{:,j}\|_2$ for $j \in \{v_x, v_y, a_x, a_y, \text{speed}\}$. For a global view, we also vectorize $\{g_k(\tau)\}_{k,\tau}$, run PCA, and scatter the first two PCs.

Figure 7 (a) shows per-input energies versus lag, revealing input selectivity and decay rates. Figure 7 (b) visualizes the geometry of vectorized impulse blocks, where marker shape represents component identity and color denotes the lag. These demonstrate that MoLDS components exhibit separated clusters corresponding to component-specific dynamical subspaces.

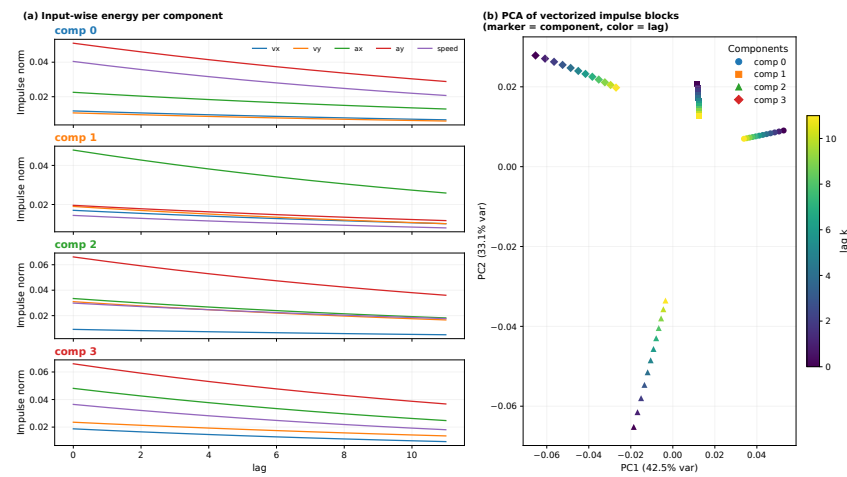


Figure 7: Input specificity and geometry of Markov responses: Left: input-wise energies versus lags are shown per component. Right: PCA of vectorized impulse blocks (marker shape = component, color = lags).